arXiv:1408.6281v1 [nucl-th] 26 Aug 2014

Nuclear pairing from microscopic forces: singlet channels and higher-partial waves

Stefano Maurizio

Department of Physics, University of Bologna, I-40126 Bologna, Italy

Jeremy W. Holt

Department of Physics, University of Washington, Seattle, WA 98195-1560

Paolo Finelli

Department of Physics, University of Bologna, I-40126 Bologna, Italy

INFN, Bologna section, I-40127 Bologna, Italy

Abstract

Background: An accurate description of nuclear pairing gaps is extremely important for understanding static and dynamic properties of the inner crusts of neutron stars and to explain their cooling process.

Purpose: We plan to study the behavior of the pairing gaps Δ_F as a function of the Fermi momentum k_F for neutron and nuclear matter in all relevant angular momentum channels where superfluidity is believed to naturally emerge. The calculations will employ realistic chiral nucleon-nucleon potentials with the inclusion of three-body forces and self-energy effects.

Methods: The superfluid states of neutron and nuclear matter are studied by solving the BCS gap equation for chiral nuclear potentials using the method suggested by Khodel *et al.*, where the original gap equation is replaced by a coupled set of equations for the dimensionless gap function $\chi(p)$ defined by $\Delta(p) = \Delta_F \chi(p)$ and a non-linear algebraic equation for the gap magnitude $\Delta_F = \Delta(p_F)$ at the Fermi surface. This method is numerically stable even for small pairing gaps, such as that encountered in the coupled ${}^3PF_2$ partial wave.

Results: We have successfully applied Khodel's method to singlet (S) and coupled channel (SD and PF) cases in neutron and nuclear matter. Our calculations agree with other *ab-initio* approaches, where available, and provide crucial inputs for future applications in superfluid systems.

PACS numbers: 21.30.-x; 21.65.-f; 26.60.-c

I. INTRODUCTION

Superfluidity in neutron matter is connected to different aspects of neutron star physics. At the surface of the star [1, 2], where a neutron gas moves in a lattice structure of neutron-rich nuclei and a sea of relativistic electrons, a $^1S_0$ neutron pairing gap naturally emerges, while at larger densities a (possibly anisotropic) $^3PF_2$ gap plays a more important role (in particular for neutron star cooling [3, 4]). At the same time, the nuclear matter case could be interesting for finite nuclear systems where neutron-proton pairing is relevant [5], even if the appearance of pairing in ordinary uniform matter is probably questionable because of known instabilities [6] which could hide superfluidity in a broad range of densities.

The goal of this article is to solve the BCS equations starting from modern nucleon-nucleon (NN) forces based on chiral effective field theory [7–9]. In this approach one identifies the appropriate low-energy degrees of freedom and derives the most general Lagrangian compatible with the symmetries and symmetry-breaking pattern of the underlying fundamental theory (i.e., QCD). The first steps towards a realistic NN potential from first principles started almost twenty years ago within the framework of Chiral Perturbation Theory (ChPT) [10, 11]. In ChPT the nuclear potential emerges naturally as a hierarchy of terms controlled by a power expansion in Q/Λ_χ, where Q is a soft scale (pion mass, nucleon momentum) and Λ_χ is a hard scale (the nucleon mass M_N or the chiral symmetry breaking scale $4\pi f_\pi$). Two-nucleon forces appear at leading order $(Q/\Lambda_\chi)^0$, while three-nucleon forces appear first at order $(Q/\Lambda_\chi)^3$, or next-to-next-to-leading order (N2LO).

We employ primarily the high-precision NN potential developed in Ref. [7] at next-to-next-to-next-to-leading order (N3LO) in the chiral expansion, but to asses theoretical uncertainties associated with the choice of cutoff scale and regulating functions, we employ in addition the chiral nuclear potentials developed in Ref. [8] in selected cases. To implement the leading three-nucleon force, we include a two-body density-dependent potential [12, 13] (see also Refs. [14–17] for other approaches and relevant details). To improve convergence in many-body perturbation theory, it is desirable to employ nuclear interactions with a cutoff scale below $\Lambda \sim 500\,\mathrm{MeV}$. One approach is to employ renormalization group (RG) methods that decouple the low- and high-momentum components of the potential. Two different methods for evolving nuclear potentials to block- and band-diagonal form in a momentum-space representation, V_{lowk} and V_{srg} respectively, have been developed (see Refs.

[18–20] for detailed reviews) and used in the present study. An alternative approach would be to construct from the beginning chiral nuclear potentials at lower cutoff scales [21–23].

The paper is organized as follows. Section II introduces the BCS theory that is the standard framework for a microscopic description of nucleonic pairing. In particular, the numerical implementation first introduced by Khodel *et al.* [24] will be reviewed. Sections III A and III B describe, respectively, our predictions for pairing gaps in the singlet and in the coupled channel cases. The role of the two-body NN interaction will be discussed along with the influence of three-body forces and self-energy effects. Finally, Section IV presents our conclusions.

II. THE BCS EQUATION

In this section we explain the method employed to solve the BCS equations [25] by partial-wave decomposition [5, 24, 26, 27]. For simplicity we largely neglect spin and isospin degrees of freedom in the derivation. The BCS equation reads in terms of the NN potential $V(\mathbf{k},\mathbf{k}') = \langle \mathbf{k}\,|V|\,\mathbf{k}'\rangle$ as follows

$$\Delta\left(\mathbf{k}\right) = -\sum_{\mathbf{k}'}\langle \mathbf{k}\,|V|\,\mathbf{k}'\rangle \frac{\Delta\left(\mathbf{k}'\right)}{2E\left(\mathbf{k}'\right)}\,, \tag{1}$$

with $E(\mathbf{k})^2 = \xi(\mathbf{k})^2 + |\Delta(\mathbf{k})|^2$ and where $\xi(\mathbf{k}) = \varepsilon(\mathbf{k}) - \mu$, $\varepsilon(\mathbf{k})$ denotes the single-particle energy and μ is the chemical potential. As in [5], we decompose the interaction

$$\langle \mathbf{k}\,|V|\,\mathbf{k}'\rangle = 4\pi \sum_{l}(2l+1)P_l(\hat{\mathbf{k}}\cdot\hat{\mathbf{k}}')V_l(k,k') \tag{2}$$

and the gap function

$$\Delta(\mathbf{k}) = \sum_{lm}\sqrt{\frac{4\pi}{2l+1}}Y_{lm}(\hat{\mathbf{k}})\Delta_{lm}(k)\,, \tag{3}$$

where $Y_{lm}(\hat{\mathbf{k}})$ denotes the spherical harmonics, l is the orbital angular momentum, m is its projection along the z axis and $P_l(\hat{\mathbf{k}}\cdot\hat{\mathbf{k}}')$ refers to the Legendre polynomials. After performing an angle-average approximation (we do not retain the m-dependence, anisotropic pairing gaps [27] will be discussed in a forthcoming paper) we have the following equation for any value of l

$$\Delta_l^j(k) = \sum_{l'}\frac{(-1)^{\Lambda}}{\pi}\int dk'\; V_{ll'}^j(k,k')\frac{\Delta_{l'}^j(k')}{E(k')}k'^2\,, \tag{4}$$

where $\Lambda = 1 + (l - l')/2$, j refers to the total angular momentum ($\vec{J} = \vec{l} + \vec{S}$) quantum number including spin $\vec{S}$ and now $E(k)^2 = \xi(k)^2 + \sum_{jl} \Delta_l^j(k)^2$. Gaps with different l and j are coupled due to the energy denominator but, for the sake of simplicity, we assume that different components of the interaction mainly act on non-overlapping intervals in density. This assumption will turn out to be correct in the neutron matter case while only partially justified when treating gaps for symmetric nuclear matter. To solve Eq. (4), we follow the approach suggested by Khodel *et al.* [24] that has been proven to be stable even for small values of the gap and to require only the initial assumption of a scale factor δ (results, of course, will be δ-independent). We define an auxiliary potential W according to

$$W_{ll'}(k,k') = V_{ll'}(k,k') - v_{ll'}\phi_{ll'}(k)\phi_{ll'}(k') \ , \tag{5}$$

where $\phi_{ll'}(k) = V_{ll'}(k,k_F)/V_{ll'}(k_F,k_F)$ and $v_{ll'} = V_{ll'}(k_F,k_F)$ so that $W_{ll'}(k,k')$ vanishes on the Fermi surface. The coupled gap equations can be rewritten as

$$\Delta_l(k) - \sum_{l'} (-1)^\Lambda \int d\tau' \ W_{ll'}(k,k') \frac{\Delta_{l'}(k')}{E(k')} = \sum_{l'} D_{ll'}\phi_{ll'}(k) \ , \tag{6}$$

where $d\tau = k^2 dk/\pi$ and the coefficients $D_{ll'}$ satisfy

$$D_{ll'} = (-1)^\Lambda v_{ll'} \int d\tau \ \phi_{ll'}(k) \frac{\Delta_{l'}(k)}{E(k)} \ . \tag{7}$$

The gap is defined as follows

$$\Delta_l(k) = \sum_{l_1 l_2} D_{l_1 l_2} \chi_l^{l_1 l_2}(k) \ , \tag{8}$$

where

$$\chi_l^{l_1 l_2}(k) - \sum_{l'} (-1)^\Lambda \int d\tau' \ W_{ll'}(k,k') \frac{\chi_{l'}^{l_1 l_2}(k')}{E(k')} = \delta_{ll_1}\phi_{l_1 l_2}(k) \ , \tag{9}$$

and $\delta_{ll'}$ is the scale factor. The property that $W_{ll'}(k,k')$ vanishes on the Fermi surface ensures a very weak dependence of $\chi_l^{l_1 l_2}(k)$ on the exact value of the gap so that, in first approximation, it is possible to rewrite the previous equation (9) as

$$\chi_l^{l_1 l_2}(k) - \sum_{l'} (-1)^\Lambda \int d\tau' \ W_{ll'}(k,k') \frac{\chi_{l'}^{l_1 l_2}(k')}{\sqrt{\xi^2(k') + \delta^2}} = \delta_{ll_1}\phi_{l_1 l_2}(k) \ . \tag{10}$$

We use this equation to evaluate $\chi_l^{l_1 l_2}(k)$ initially by matrix inversion, then we use this function to self-consistently evaluate $D_{ll'}$. Finally, we solve the system given by Eqs. (7)–(9)

in a self-consistent procedure. We always assume $\mu = \varepsilon_F$ and adopt the relativistic version of the single-particle energy $\varepsilon(k) = \sqrt{k^2 + M_N^2}$, where M_N is the nucleon mass. In principle, the effective force to be included in Eq. (1) should be generated by the sum of all particle-particle irreducible Feynman diagrams [28], but in most applications to nuclear systems only the bare nucleon-nucleon interaction is kept [5]. Corrections to the bare force, caused by medium polarization effects (see Refs. [29–31] and references therein) will be neglected in the present analysis and postponed to a forthcoming paper. As a consequence, for the pairing potential $V(p,k)$ we introduce the following ansatz:

$$V(p,k) = V_{2B}(p,k) + V_{3B}(p,k,m) \simeq V_{2B}(p,k) + V_{2B}^{eff}(k_F,p,k) \; , \tag{11}$$

where V_{2B} is the Idaho [7] NN potential at N3LO in the chiral expansion[1] or the Juelich version [8], and the three-body potential is approximated by an effective two-body density-dependent potential V_{2B}^{eff} derived by Holt *et al.* in Refs. [12, 13]. We employ in our calculations the evolved two-body potentials $V_{\rm lowk}$ (with a smooth cut-off in momentum space [33]) and $V_{\rm srg}$ [19] using two different evolution operators (see Sect. III B for more details). When considering self-energy effects, we simply perform the transformation $M_N \to M_N^*$ using the effective mass obtained by Holt *et al.* in Ref. [34] using a density matrix expansion technique. In Ref. [34] the two-body interaction was comprised of long-range one- and two-pion exchange contributions and a set of contact terms contributing up to fourth power in momenta as well as the leading order chiral three-nucleon interaction. The explicit formula is given by

$$M^*(\rho) = M\left(1 + 2MF_\tau(\rho) - \frac{k_F^2}{2M^2}\right)^{-1} \; , \tag{12}$$

where the strength function $F_\tau(\rho)$ is defined as follows

$$F_\tau(\rho) = \frac{1}{2k_F}\left(\frac{\partial U(p,k_F)}{\partial p}\right)_{p=k_F} \tag{13}$$

with $U(p,k_F)$ the single particle potential and $-\frac{k_F^2}{2M^2}$ a relativistic correction. In Fig. 1 we plot the effective masses for nuclear and neutron matter as functions of density. From the effective mass behavior we can expect that the self-energy effects will play a central role in the high-density components of the gap, while at low densities the effects will be rather negligible. Second-order perturbative contributions to the single-particle energies are expected to increase the effective mass [35].

[1] Among the different versions, we employ the chiral potential in which the regulator function $f(p',p) = \exp[-(p'/\Lambda)^{2n} - (p/\Lambda)^{2n}]$ has the cutoff $\Lambda = 500\,\mathrm{MeV}$, and $n = 2$ for the 2π exchange contributions [32].

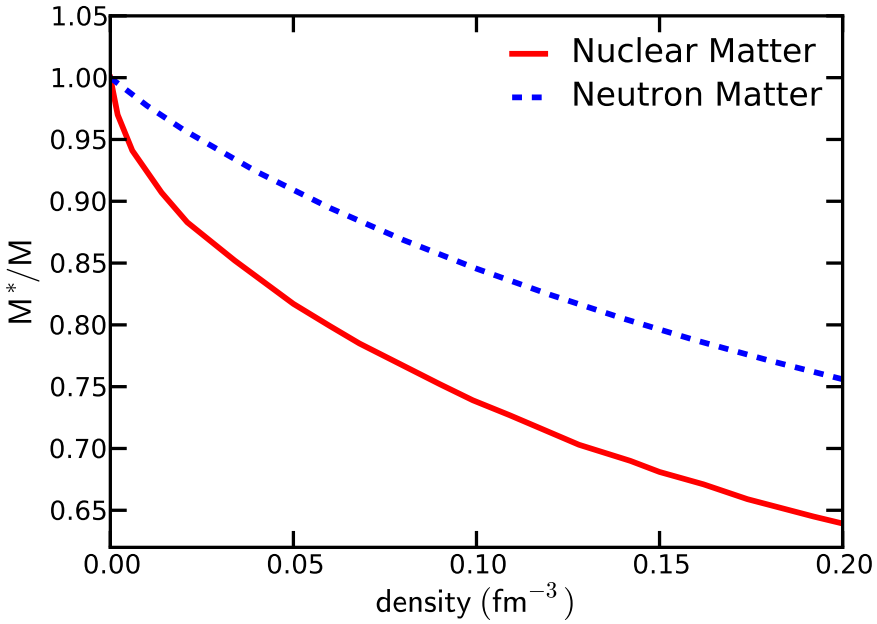

FIG. 1. (color online) The effective mass in the case of nuclear (red line) and neutron (blue dashed line) matter as a function, respectively, of the total nucleon density ρ or the neutron density ρ_n (see Ref. [34]) .

III. PAIRING GAPS

A. Singlet channel ($^1S_0$)

In the singlet channel, the only difference between the nn and np potential is the charge independence breaking and the charge symmetry breaking terms, which are treated as small perturbations in ChPT. In Fig. 2 we test our solution to the gap equation, in the nuclear matter case, against previously published results [36] with the low-momentum interaction $V_{\rm lowk}$. In addition, we compute the $^1S_0$ gap from the bare chiral NN interaction and find a qualitatively very similar behavior. The gap Δ_F reaches a maximum value of approximately 3.5 MeV at $k_F \simeq 0.85\,{\rm fm}^{-1}$ when the bare interaction is used in the two-body sector, while a somewhat reduced gap (by almost 0.5 MeV) if we consider $V_{\rm lowk}$.

In the neutron matter case, at the two-body level, there is good agreement with the gap computed from well known realistic potentials like the CD-Bonn or Nijmegen interactions

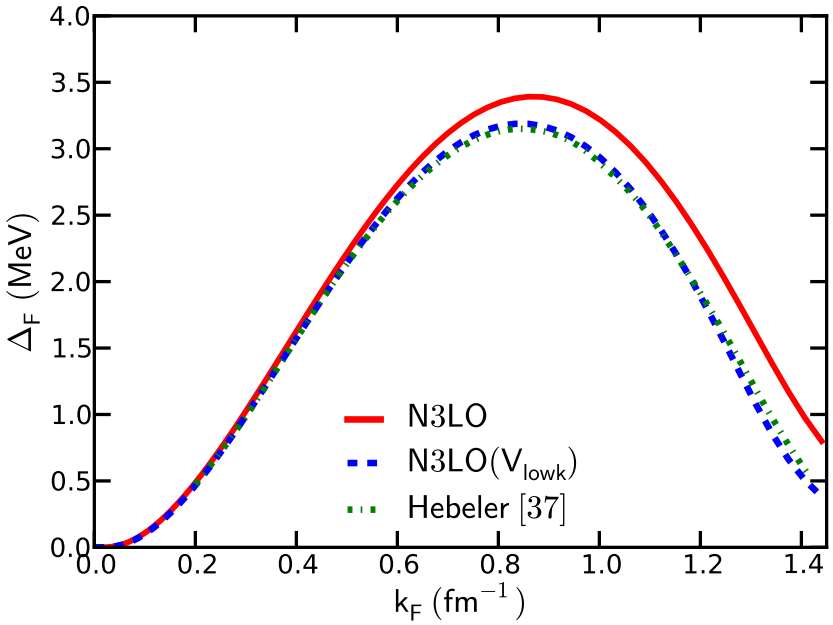

FIG. 2. (color online) The $^1S_0$ gap for nuclear matter computed with the realistic chiral potential of Ref. [7, 32] at N3LO (red line) and the corresponding $V_{\rm lowk}$ potential (blue dashed line). With the green dashed-dotted line we include, as a benchmark, a similar calculation performed by Hebeler *et al.* [36].

[5, 37, 38], but at larger densities the N3LO gap exhibits a higher value. This can be explained by observing that the phase shifts from the chiral N3LO potential exhibit more attraction than the CD-Bonn potential for high momenta, as already observed by Hebeler *et al.* [36]. In Fig. 3 we compare our full calculation for the gap, i.e., with the complete potential in Eq. (11) and the density-dependent effective mass in Eq. (12), with recent results by Hebeler *et al.* [36], where the authors started from a chiral N3LO interaction and evolved to a sharp low-momentum interaction[2]. Also presented for comparison are *ab-initio* results obtained in the last several years: Auxiliary Field Diffusion Monte Carlo (AFDMC) [39] with AV8' [40] + UIX [41] potentials, Quantum Monte Carlo (QMC) [42], where the authors have retained the S-wave part of the AV18 [43] interaction, and Correlated Basis Functions (CBF) [44] still with AV8' plus UIX. We observe that at low densities the gap

[2] We used a rather different approach to construct our $V_{\rm lowk}$. The RG procedure has been performed with different cutoffs and regulating functions, in particular a Fermi-Dirac function $f_\Lambda(k) = 1/(1+e^{(k^2-\Lambda^2)/\varepsilon^2})$ and an exponential cutoff $f_\Lambda(k) = e^{-(k^2/\Lambda^2)^n}$ [33]. The results show a very weak cutoff-dependence.

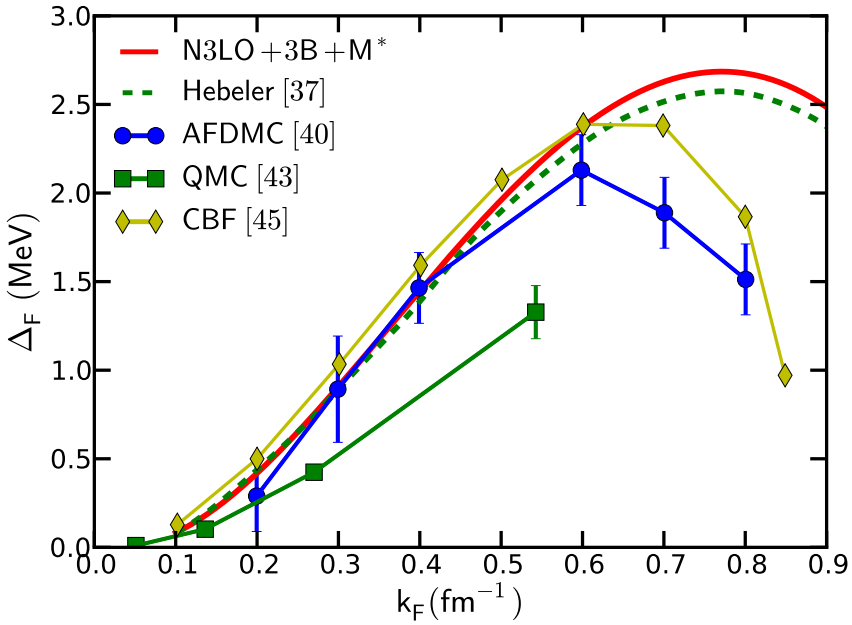

FIG. 3. (color online) The $^1S_0$ gap for neutron matter computed with the realistic chiral potential of [7, 32] at N3LO plus the three-body contribution of Eq. (11) and the inclusion of the effective mass in Eq. (12). As a comparison, we include a similar calculation by Hebeler [36] with a green dashed line and a set of *ab-initio* simulations with different many-body techniques: AFDMC (blue circles) [39], QMC Green Functions (green squares) [42] and CBF (yellow diamonds) [44]. See the text for additional details.

behaviors are very similar, but beyond Fermi momenta of $k_F \approx 0.6$ fm^{-1} the gaps computed with the Argonne potentials decrease rapidly in contrast to those from chiral interactions. At the present time, it is hard to assess if disagreement is due to different choices in the nuclear Hamiltonian or different many-body methods.

It is useful to consider separately the different physical effects governing the $^1S_0$ pairing gap. In Fig. 4 we plot the gaps obtained with two-body interactions alone (the dotted lines represent the bare and the renormalized N3LO potentials), with the inclusion of effective three-body forces (dashed lines) and considering also self-energy effects (solid lines). By construction, we expect that at low densities the three-body effects are rather small, while only at higher densities do they become appreciable. The main role of both three-body forces and the effective mass is to substantially reduce the attractive strength in the S channel (for

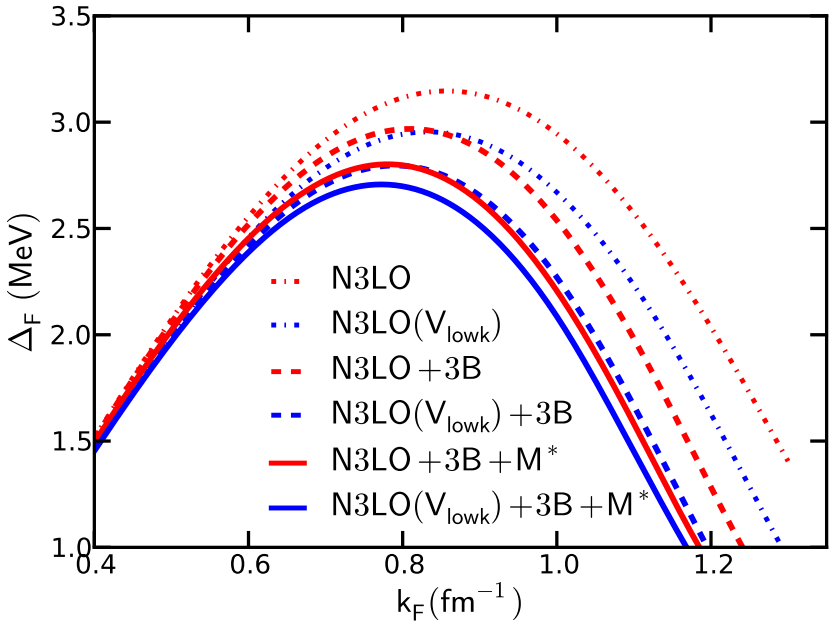

FIG. 4. (color online) The $^1S_0$ gap for neutron matter. In this figure we show all the contributions to the pairing gap Δ_F starting from the inclusion of the bare two-body potential (red dotted line) or $V_{\rm lowk}$ (blue dotted line) and then including effective three-body forces (dashed lines) and a density-dependent effective mass (solid lines).

higher partial waves the situation is more involved, see Sect. III B).

B. Higher partial waves ($^3SD_1$ and $^3PF_2$)

In addition to the $^1S_0$ channel, in the nuclear matter case a non-vanishing gap appears in the $^3SD_1$ channel. The presence of a bound state in this channel and the very high phase shifts in the $^3S_1$ channel indicate that the interaction is more attractive than in the other channels. As a consequence the gap has a magnitude of about 10 MeV, as can be seen in Fig. 5, with conventional realistic potentials. There is no agreement on the details of the gap in this channel, but both Elgarøy *et al.* [45] and Takatsuka *et al.* [26] suggest the possibility of a gap of such magnitude (see curves labeled, respectively, by BONN-A and OPEG in Fig. 5). While BONN-A [46] is a complete one-boson exchange potential, OPEG [26] contains only the one-pion exchange tail and a Gaussian repulsive core. The combined

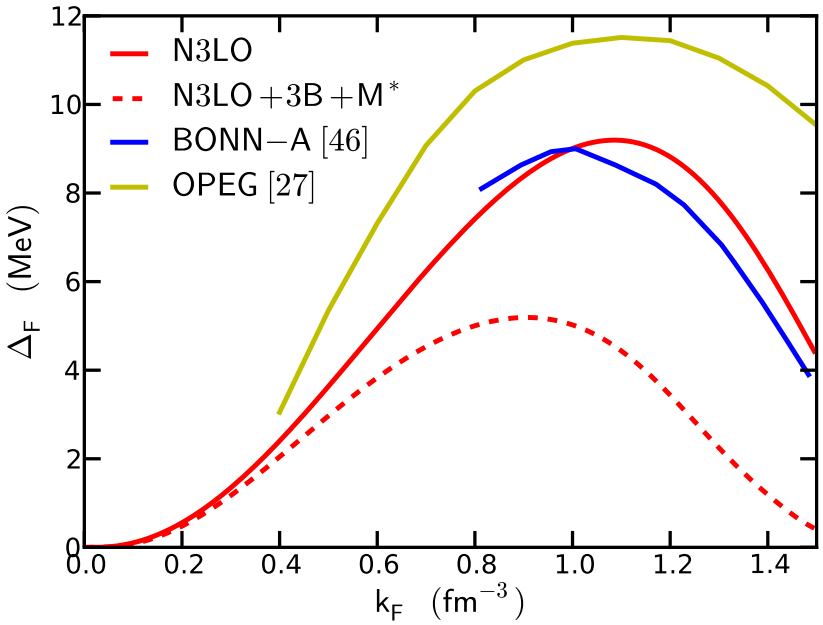

FIG. 5. The gap in the ${}^3SD_1$ channel. We plot our calculations with the N3LO interaction (red line) in comparison with results obtained employing BONN-A potential [45] (blue curve) and OPEG [26] (yellow line). All results suggest a very large pairing gap (around 10 MeV), but complete calculations including three-body forces and effective masses (see Eqs. (11) and (12)), shown in the dashed red curve, indicate a substantial reduction and a sizable modification of the gap's shape.

effect of three-body forces and self-energy effects leads not only to a sizable reduction of the gap itself but also to a shift of the gap's maximum at $k_F \approx 1$ fm^{-1} and a rapid decrease at higher Fermi momenta.

Due to the large densities over which the pairing gap remains finite, it is questionable whether low-momentum interactions, $V_{\rm lowk}$, with a block-diagonal momentum-space cutoff on the order of $\Lambda \sim 2.0\,{\rm fm}^{-1}$ are appropriate. A better approach is provided by the Similarity Renormalization Group (SRG), where off-diagonal momentum-space matrix elements are supressed. In this case, we study nuclear Hamiltonians $H = T_{rel} + V$ evolved through the SRG procedure [19], where we define a class of Hamiltonians

$$H_s = U_s H U_s^\dagger \equiv T_{rel} + V_s \tag{14}$$

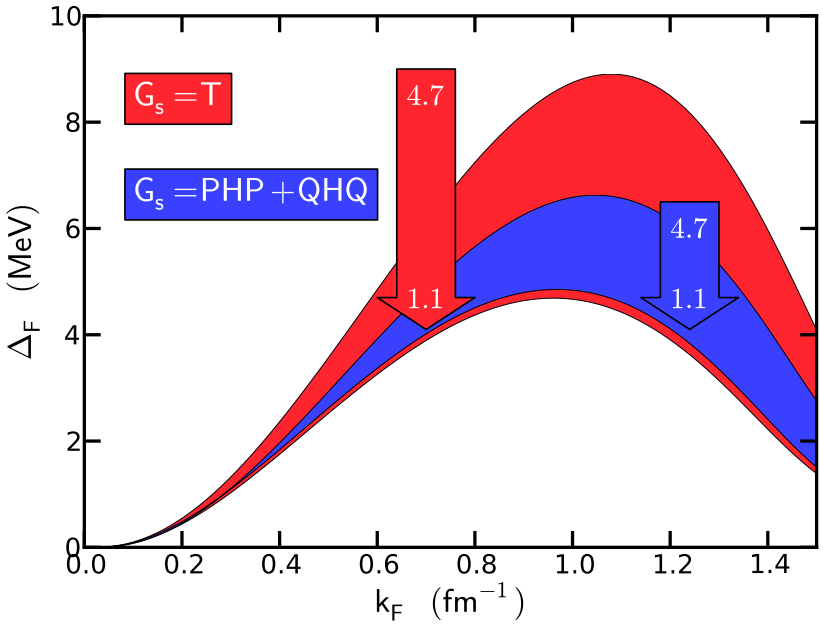

FIG. 6. (color online) The evolution of the pairing gap in the ${}^3SD_1$ channel with SRG-evolved interactions. We employed two different evolution operators $G_s : T_{rel}$ (red band) and $PHP+QHQ$ (blue band). The arrows denote the flow variable λ (related to s through $\lambda \equiv s^{-1/4}$) which is varied from 4.7 fm $^{-1}$ down to 1.1 fm^{-1}.

with a generator

$$\eta_s = \frac{dU_s}{ds} U_s^\dagger = -\eta_s^\dagger \, . \tag{15}$$

If we choose $\eta_s = [G_s, H_s]$ the flow equation takes the form

$$\frac{dH_s}{ds} = [[G_s, H_s], H_s] \ . \tag{16}$$

As shown in [19], results obtained from SRG-evolved interactions are very similar to those obtained from $V_{\rm lowk}$ if an appropriate G_s is chosen. Moreover, the SRG interaction has many salient features of low-momentum interactions, such as independence of the physical observables from the operator G_s, perturbativeness and universality. In the literature it is common to encounter also the dimensional parameter $\lambda = s^{-1/4}$ fm^{-1}. A very interesting feature of the SRG procedure is that the tensor interaction strength is reduced as s increases, and this modification to the interaction can strongly modify the ${}^3SD_1$ gap. Since all physical observables should remain unchanged under an SRG transformation, this variation represents an

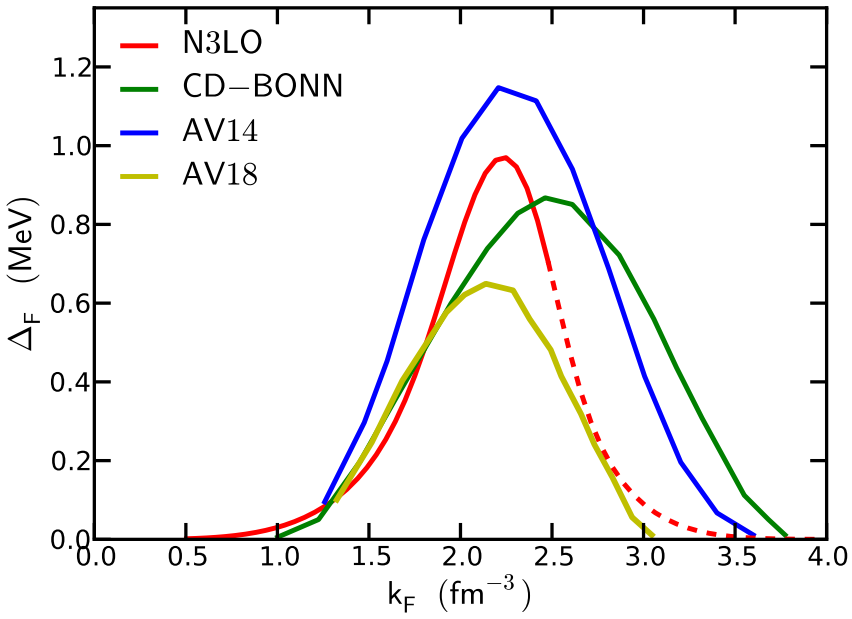

FIG. 7. (color online) The gap in the ${}^3PF_2$ channel obtained from the N3LO [32] (red line) interaction in comparison with several realistic NN potentials taken from Ref. [5]. Chiral potentials, by definition, can be trusted only up to momenta close to the cutoff (beyond the cutoff, the pairing gap is symbolized with a dashed line).

uncertainty estimate in the pairing strength. A common choice for G_s is T_{rel}, and in this case as s increases, V_s approaches the diagonal form. We tested one more generator

$$G_s = P_\Lambda H_s P_\Lambda + Q_\Lambda H_s Q_\Lambda \ , \tag{17}$$

where P_Λ and Q_Λ are, respectively, the projector and the exclusion operators in the subspace $\{k < \Lambda\}$ (see Sect. 3.4 in Ref. [19]). From Eq. (16) it is easy to see that, if H is a two body Hamiltonian expressed in the second quantization formalism, $(dH_s/ds)_{s=0}$ will also include three body interactions. In this way, the evolution over the flow will naturally induce many-body interactions. The errors arising from omitting the induced many-body forces can be estimated by analyzing the dependence of the physical observables on the flow parameter λ. Our results are shown in Fig. 6, where we tested the two evolution operators. For $G_s = T_{rel}$ (red color) we found that the gap becomes quite stable for $\lambda < 2.2$ fm^{-1}, where the maximum is reduced to approximately 5 MeV (a factor of 2 smaller compared

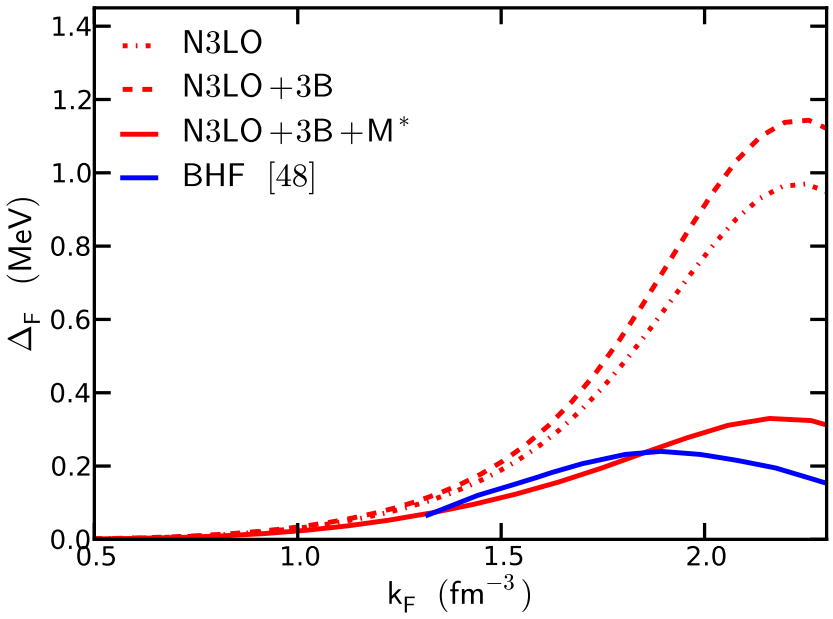

FIG. 8. (color online) The gap in the ${}^3PF_2$ channel with only N3LO potential (dotted red line), with three-body forces (dashed red line) and including also self-energy effects (solid red line). In comparison we plot the results of recent BHF calculations [47] (blue curve).

to the bare potential). In the range 1.3 fm$^{-1} \leq \lambda \leq 2.2$ fm^{-1} the variation in the size of the gap is on the order of 0.5 MeV or less. When using G_s given by Eq. (17) we obtained very similar results, confirming the approximate independence of the physical results on the choice of G_s, but with a reduced cutoff-dependence.

In the neutron matter case, while at low density the dominant channel is the ${}^1S_0$ partial wave, at higher densities the high-momentum components (which are repulsive) become more important, suppressing the gap, and this happens at $k_F \approx 1.5$ fm^{-1}. At these densities, the only channel which substantially contributes to the neutron matter gap is the coupled ${}^3PF_2$, where the coupling is due to the tensor interaction. As can be seen in Fig. 7, there is a significant dependence of the gap on the potential model, though the peak in the gap consistently occurs between $2.2 \leq k_F \leq 2.6$ fm^{-1}. At the high densities and associated momentum scales relevant for pairing in this channel, realistic NN interactions are not as well constained by fits to phase shifts, which partially explains the differences in the observed gaps. As explained in [7], in this channel one expects a crucial contribution from the three-

pion-exchange topology at N^{4}LO and from the contact term at N^{5}LO, which should reduce the attraction in this channel. All reasonable interactions give a gap of magnitude ≈ 1 MeV, and we expect a small but not negligible reduction of the gap from the higher orders in Q/Λ_χ. In Fig. 8 we plot predictions for the $^3PF_2$ gap including three-body forces (dashed red line) and self-energy effects (solid red line) in comparison with a very recent Brueckner-Hartree-Fock calculation by Dong *et al.* [47], where the authors employed the Bonn B potential [48] and a microscopic three-body force constructed by Li *et al.* [49]. Our complete calculation nicely agrees with [47], in particular for small momenta, and suggests a sizeable reduction of the gap if many-body forces are taken into account.

In Fig. 9 we show also the $^3PF_2$ gap we have computed from the Juelich ChPT potentials [8]. Because the $^3PF_2$ gap extends towards very large densities (even beyond the reasonable limits of applicability of a ChPT approach) is very interesting to test the robustness of previous calculations (see Figs. 7 and 8) against a different theoretical approach. In fact, in the last years Epelbaum *et al.* developed a new scheme in the construction of a realistic chiral potential where, instead of a Dimensional Regularisation scheme for chiral-loop integrals, a finite cutoff Λ is kept in the range of $500 - 800$ MeV which appears to be physically reasonable and matches well with the cutoff used in the Lippmann-Schwinger (LS) equation. As a consequence, in our calculations we employed two different cutoffs: Λ_{LS} for the LS equation (with non relativistic kinematics) and $\Lambda_{2\pi}$ for the spectral-function regulator (SFR) of the two-pion exchange potential (varied between 500 and 700 MeV). For Fermi momenta up to nearly $k_F = 1.4$ fm^{-1}, the predictions from the different potentials are nearly universal and agree reasonably well with the predictions from the Entem and Machleidt chiral N3LO potential. However, beyond this density there is a significant scale dependence in the theoretical predictions, in particular to $\Lambda_{2\pi}$. This uncertainty has to be taken into account if microscopic $^3PF_2$ gaps are used to describe the cooling process of neutron stars [50].

IV. CONCLUSIONS

We have presented calculations of the pairing gaps in infinite nuclear and neutron matter employing realistic two- and three-body nuclear forces derived within the framework of chiral effective field theory. The BCS gap equation is solved employing Khodel's method, which is found to be stable even for small values of the pairing gap. Three-nucleon forces help reduce

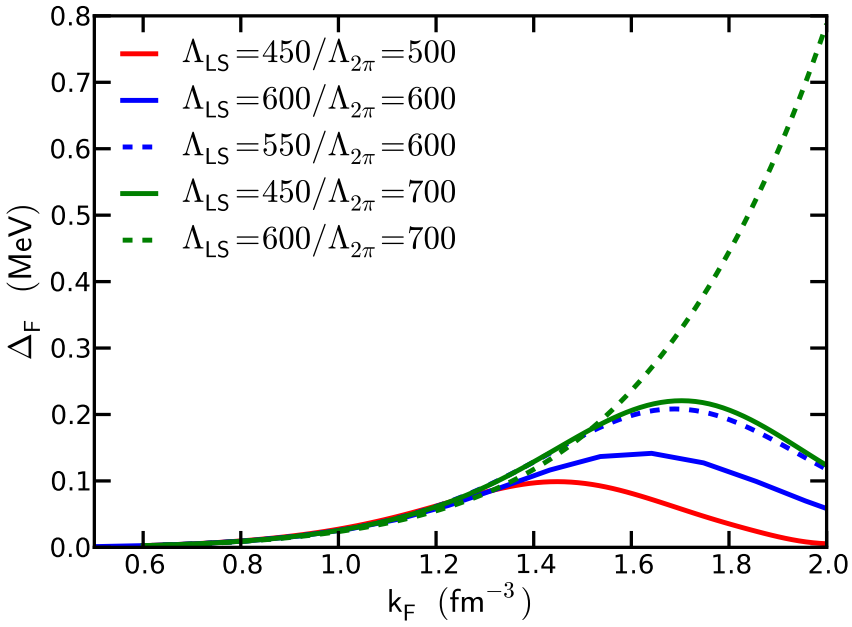

FIG. 9. The gap in the ${}^3PF_2$ channel as a function of the resolution scale in the Juelich nucleon-nucleon interactions [8]. The scales refer respectively to the cutoffs (units of MeV) in the Lippmann-Schwinger equation (Λ_{LS}) and the spectral function regulator in multi-pion exchange loop diagrams($\Lambda_{2\pi}$). It appears that the magnitude of the gap's maximum is very sensitive to $\Lambda_{2\pi}$ and, to a lesser content, to Λ_{LS}.

the strength of pairing in the ${}^1S_0$ and coupled ${}^3SD_1$ channels, while for the coupled ${}^3PF_2$ channel the three-nucleon forces enhances the gap. In all cases considered in the present work, consistent nucleon effective masses reduce pairing correlations. Of particular interest is the scale dependence of the ${}^3PF_2$ pairing gap, which exhibits a nearly universal behavior at low densities in all chiral potentials considered. This works sets the stage for future applications to pairing gaps in finite-temperature neutron matter [50].

V. ACKNOWLEDGEMENTS

Work supported in part by US DOE Grant No. DE-FG02-97ER-41014. The authors are deeply grateful to E. Epelbaum (Institut für Theoretische Physik II, Ruhr-Universität

Bochum) for providing the chiral potential of Ref. [8].

---

[1] P. Haensel, A. Y. Potekhin and D. G. Yakovlev, *Structure and Equation of State of Neutron Star Crusts*, published in *Neutron Stars 1* (2007) 115, Springer New York.

[2] N. Chamel and P. Haensel, Living Rev. Relativity **11** (2008) 10.

[3] D. Page, M. Prakash, J. M. Lattimer and A. W. Steiner, Phys. Rev. Lett. **106** (2011) 081101.

[4] D. Page, J. M. Lattimer, M. Prakash and A. W. Steiner, `arXiv:1302.6626`, to be published in the book *Novel Superfluids*, Eds. K.H. Bennemann and J.B. Ketterson".

[5] M. Hjorth-Jensen and D. J. Dean, Rev. Mod. Phys. **75** (2003) 607.

[6] J. M. Lattimer and D. G. Ravenhall, Astr. J. **223** (1978) 314.

[7] R. Machleidt and D. R. Entem, Phys. Rept. **503** (2011) 1 and references therein.

[8] E. Epelbaum, H.-W.Hammer and Ulf-G. Meissner, Rev. Mod. Phys. **81** (2009) 1773 and references therein.

[9] S. Weinberg, Physica A **96** (1979) 327.

[10] C. Ordóñez and U. van Kolck, Phys. Lett. B **291** (1992) 459.

[11] V. Bernard, N. Kaiser, Ulf-G. Meissner, Int. J. Mod. Phys. E **4** (1995) 193.

[12] J. W. Holt, N. Kaiser and W. Weise, Phys. Rev. C **79** (2009) 054331.

[13] J. W. Holt, N. Kaiser and W. Weise, Phys. Rev. C **81** (2010) 024002.

[14] K. Hebeler and A. Schwenk, Phys. Rev. C **82** (2010) 014314.

[15] T. Lesinski, K. Hebeler, T. Duguet and A. Schwenk, J. Phys. G: Nucl. Part. Phys. **39** (2012) 015108.

[16] S. Gandolfi, A. Y. Illarionov, K. E. Schmidt, F. Pederiva and S. Fantoni, Phys. Rev. C **79** (2009) 054005.

[17] A. Lovato, O. Benhar, S. Fantoni, A. Y. Illarionov and K. E. Schmidt, Phys. Rev. C **83** (2011) 054003.

[18] S. K. Bogner, T. T. S. Kuo and A. Schwenk, Phys. Rept. **386** (2003) 1.

[19] S. K. Bogner, R. J. Furnstahl and A. Schwenk, Prog. Part. Nucl. Phys. **65** (2010) 94 and references therein.

[20] `http://www.physics.ohio-state.edu/~ntg/srg/`

[21] L. Coraggio, A. Covello, A. Gargano, N. Itaco, D. R. Entem, T. T. S. Kuo, and R. Machleidt, Phys. Rev. C **75** (2007) 02431.

[22] L. Coraggio, J. W. Holt, N. Itaco, R. Machleidt and F. Sammarruca Phys. Rev. C **87** (2013) 014322.

[23] L. Coraggio, J. W. Holt, N. Itaco, R. Machleidt, L. E. Marcucci and F. Sammarruca, Phys. Rev. C **89** (2014) 044321.

[24] V. V. Khodel, V. A. Khodel and J. W. Clark, Nucl. Phys. A **598** (1996) 390.

[25] J. Bardeen, L. N. Cooper and J. R. Schrieffer, Phys. Rev. C **38** (1957) 1175; J.R. Schrieffer, *Theory of the Superconductivity*, Benjamin, New York, 1964.

[26] T. Takatsuka and R. Tamagaki Progr. Theor. Phys. Suppl. **112** (1993) 27.

[27] V. V. Khodel, V. A. Khodel and J. W. Clark, Nucl. Phys. A **679** (2000) 827.

[28] A. B. Migdal, *Theory of finite Fermi systems and applications to atomic nuclei*, Interscience, New York (1967).

[29] H. J. Schulze, J. Cugnon, A. Lejeune, M. Baldo and U. Lombardo, Phys. Lett. B **375** (1996) 1.

[30] U. Lombardo, H. Schulze, C.-W. Shen and W. Zuo, Int. J. Mod. Phys. E **14** (2005) 513.

[31] M. Baldo, U. Lombardo, S. S. Pankratov and E. E. Saperstein, J. Phys. G **37** (2010) 064016.

[32] D. R. Entem and R. Machleidt, Phys. Rev. C **68** (2003) 041001(R).

[33] S. K. Bogner, R. J. Furnstahl, S. Ramanan and A. Schwenk, Nucl. Phys. A **784** (2007) 79.

[34] J. W. Holt, N. Kaiser, and W. Weise, Eur. Phys. J. A **47** (2011) 128.

[35] J. W. Holt, N. Kaiser, G. A. Miller and W. Weise, Phys. Rev. C **88** (2013) 024614.

[36] K. Hebeler, A. Schwenk and B. Friman, Phys. Lett. B **648** (2007) 176.

[37] R. Machleidt, Phys. Rev. C **63** (2001) 024001.

[38] Th. A. Rijken and V. G. J. Stoks, Phys. Rev. C **54** (1996) 2851; Phys. Rev. C **54** (1996) 2869.

[39] S. Gandolfi, A. Y. .Illarionov, F. Pederiva, K. E. Schmidt and S. Fantoni, Phys. Rev. C **80** (2009) 045802.

[40] R. B. Wiringa and S. C. Pieper, Phys. Rev. Lett. **89** (2002) 182501.

[41] S. C. Pieper, V. R. Pandharipande, R. B. Wiringa and J. Carlson, Phys. Rev. C **64** (2001) 014001.

[42] A. Gezerlis and J. Carlson, Phys. Rev. C **77** (2008) 032801(R).

[43] R. B. Wiringa, V. G. J. Stoks and R. Schiavilla, Phys. Rev. C **51** (1995) 38.

[44] A. Fabrocini, S. Fantoni, A. Y. Illarionov and K. E. Schmidt, Phys. Rev. Lett. **95** (2005) 192501.

[45] Ø. Elgarøy, L. Engvik, M. Hjorth-Jensen and E. Osnes, Phys. Rev. C **57** (1998) R1069.

[46] R. Machleidt, Adv. Nucl. Phys. **19** (1989) 185.

[47] J. M. Dong, U. Lombardo and W. Zuo, Phys. Rev. C **87** (2013) 062801.

[48] R. Machleidt, K. Holinde and Ch. Elster, Phys. Rep. **149** (1987) 1.

[49] Z. H. Li, U. Lombardo, H.-J. Schulze and W. Zuo, Phys. Rev. C **77** (2008) 034316.

[50] S. Maurizio, J. W. Holt and P. Finelli, *Finite temperature pairing gaps from realistic forces and applications to the neutron star cooling process*, in preparation.